

OPTIMIZATION OF DISTRIBUTED BRAGG'S REFLECTORS FOR THIN-FILM AMORPHOUS SILICON SOLAR CELLS

S. Saravanan and R.S. Dubey

Advanced Research Laboratory for Nano materials & Devices, Department of Nanotechnology,
Swarnandhra College of Engineering & Technology, Seetharampuram, Narsapur-534280,
West Godavari (AP), India

ABSTRACT

In this paper, we present the light trapping mechanism of thin-film amorphous silicon (a-Si) solar cells by using rigorous coupled wave analysis (RCWA) method. Using optical modeling, the distributed Bragg's reflectors (DBR) are optimized which consists of alternative layers of silicon (Si) and silicon di-oxide (SiO₂) materials. The optical reflectivity of DBR layers was investigated from 110 DBR by changing various center wavelengths such as 400, 600, 800 and 1000 nm. The obtained results showed higher, broader and red shift reflectivity (photonic band gap) with respect to thickness and incident wavelength. Further extended and studied the new conformal thin-film solar cell architecture which includes nanogratings (top-ITO and bottom-Ag) and optimized DBR used as back reflector. The DBRs and bottom nanogratings helps to fold back the shorter and longer wavelength of light towards the absorber region with diverse and enhanced photon path length. Under normal radiation, collection of the photons and an electron-hole pair generation are enhanced in thin absorber regions, resulting highest current density of 25.16 mA/cm². Furthermore, this device implementation could be fabricated by economically.

KEYWORDS

Light trapping, silicon, RCWA, DBR, back reflector

1. INTRODUCTION

The thin film solar cell is promising and leading the photovoltaic market. The primary material and highest conversion cell efficiency mainly depend on the silicon based materials like crystalline silicon (c-Si) [1], amorphous silicon (a-Si) [2], polycrystalline silicon (p-si) and micro-crystalline (μ - Si) silicon [3] due to the natural abundance and well suited to the advanced technology. Thin film technology has disadvantages such as low cell efficiency in longer (infrared) spectral region. This issue could be solved by novel structures and useful for the better light trapping scheme (textured) which needs to be controlled the improvement of the light absorption. Because of this issue, one- dimensional (1D) photonic crystals, two-dimensional (2D) photonic crystals and three-dimensional (3D) photonic crystals are playing pivotal role in various Opto-electronic applications like solar cells. *Lee et al. and Fink et al.* found 1D photonic crystal fulfilled the required omni-directional reflector rather than the 2D-and 3D photonic crystals [4-5]. Recently, 1D photonic crystal has received a considerable performance in solar cells. To improve the light harvesting and collection of the photons, various nanostructures are used, for example antireflection coatings (ARC), one- dimensional photonic crystals (1DPCs), metallic (or dielectric) nanorods, dielectric/metallic nanogratings, nanoparticles have been proposed by

various researchers [6-10]. Among these nanostructures, 1D photonic crystals/distributed Bragg reflector (DBR), dielectric and metallic nanogratings had shown the promising absorption. Presently, the multiple nanogratings are playing important role in solar cells and garnering great attention by the various researchers [11]. *Tahmineh Jalali* presented thin film crystalline silicon solar cells with a backside reflector of DBR (Si/SiO₂), dielectric nanogratings by using a 2D-finite element method (FEM). This cell structure yielded the highest current density of 24.51 mA/cm² within 1 μm silicon absorber region [12]. *Soman and Antony* demonstrated the tunable and spectrally selective 1DPC as a backside reflector integrated amorphous silicon solar cell. With the effect (1DPC) of silicon oxy-nitrate and silicon rich silicon nitride, the highest current density of 14.77 mA/cm² was achieved in a 200 nm thick amorphous silicon absorber region [13]. *Yu et al.*, experimentally demonstrated the efficient and highly transmittance semi-transparent polymer (P3HT: ICBA) solar cells with 1DPCs (WO₃/LiF) acted as backside reflectors. They achieved the highest power conversion efficiency of 4.12% with 80 nm absorber region [14]. *Sheng et al.*, studied the light trapping mechanism in thin-film silicon solar cells by integration of 5DBR (a-Si/SiO₂) layers by the finite - difference time-domain (FDTD) method. Under transverse electric (TE) polarization, achieved 20% of cell efficiency (η) within 1.5 μm thick absorber region under 800 nm center wavelength (λ_c) with the photonic textures [15]. *Sheng et al.*, investigated thin film silicon solar cells with integration of 5DBR (SiO₂/a-Si) and nanogratings. Under the center wavelength of 800 nm (λ_c, TE case), the maximum current density of 2.95 mA/cm² reached within 1.5 μm thick silicon absorber layer [16]. *Kuo et al.*, studied the quantum efficiency enhancement of transparent hydrogenated amorphous silicon thin film solar cells by integration of 3DBR (TiO₂/SiO₂) as backside reflectors for building integrated photovoltaic devices. Overall, the external quantum efficiency enhancement of 14.7% as compared to the reference solar cell structure [17]. *Saravanan and Dubey* numerically investigated on ultrathin film crystalline silicon solar cells by integrating 1DPC as backside reflector. They demonstrated the photonic band gap reflectivity and the field intensity of 1DPC using plane wave method and rigorous coupled wave analysis (RCWA) method. Further, optimal 1DPCs used as a backside reflector in crystalline silicon solar cell and achieved the highest current density of 19.69 and 25.54 mA/cm² in both (TE and TM) polarization conditions [18]. In this letter, we focused an improvement of light trapping in thin film amorphous silicon solar cells by integration of front ITO-nanogratings, triangular bottom (Ag) nanogratings and DBRs (Si/SiO₂) as backside reflector. This engineering scheme is expected to improve the light photon path-length, lifetime and finally generated the better conversion cell efficiency (16.5%) and current density (25.16 mA/cm²) which was not reported within the 40 nm thick amorphous silicon absorber region under the transverse electric (TE) field polarization mode.

In this work, thin film amorphous silicon solar cells investigated by using RCWA method. This proposed solar cell structure systematically studied the influence of various DBR layers and nanogratings in solar cells. Next, DBR layers are optimized by changing different center wavelength of 400, 600, 800 and 1000 nm. The adoption of metallic nanogratings and optimal DBR reflector is favorable to enhance absorption in longer wavelength.

2. DESIGNING APPROACH

In the simulation, a commercial RCWA method used which was provided by RSoft synopsis software tool. The schematic diagram of the simulation model is shown in **figure 1(a)**. The DBR layers consist of two alternative materials by maintaining higher refractive index contrast like silicon (Si, n_H=3.5) and silicon dioxide (SiO₂, n_L=1.45) [18]. The maximum incidence light reflected range also known as the photonic band gap (PBG). This silicon based materials (Si and SiO₂) are abundant in nature [12]. The refractive indices is defined (or calculated) as:

$$n_i = \frac{\gamma \lambda}{4\pi} \quad (1)$$

Here, the ‘ λ ’ is the wavelength; ‘ γ ’ is an exponential loss coefficient. The periodic multilayers and highest refractive indexed materials are useful for the broader photonic band gap reported by *Zhang et al. (1994)*. They found good agreement between the numerically simulated and experimentally fabricated structures [19-22]. Consequently, the geometric thickness of the two alternative layer thickness calculated by quarter-wave equations,

$$d_i = \frac{\lambda c}{4n_i} \quad (2)$$

where, ‘ n_i ’ is the refractive index of the materials, ‘ λc ’ is the center wavelength of the incident light [16]. Using quarter wave criterion (equ. 2), the thickness of the Si and SiO₂ layers calculated with respect to the incidence wavelength and the lattice constant as tabulated in **table 1**. The designing one-dimensional photonic crystals are starts with respect to the selection of the center wavelength ($\lambda c=400, 600, 800$ and 1000 nm), refractive index (n) of the materials and a number of multilayers.

In this numerical simulation includes boundary conditions such as periodic boundary conditions (PBC) in x and y-axis. This boundary condition chooses at equivalent to infinite structures. Next, the perfect match layer (PML) in z-axis, which is useful to eliminate the outward propagating energy that impinging on the boundaries.

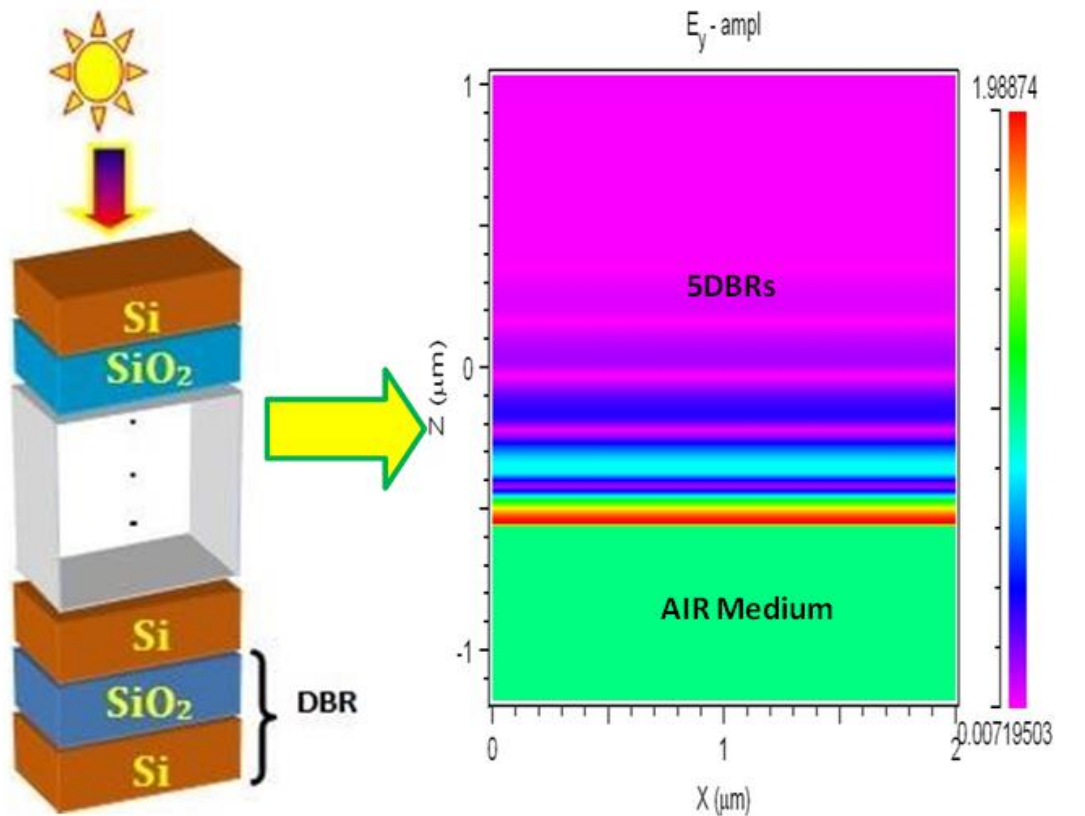


Fig. 1. The schematic diagram of Si/SiO₂ DBR stacks and field distribution.

Table 1. The thickness of the Si/SiO₂ layers at different center wavelengths.

S.N.	Center Wavelength ' λ_c ' (nm)	Thickness of DBR (Si/SiO ₂) (nm)	Lattice Constant 'a' (nm)
1	400	28 / 69	97
2	600	42/103	145
3	800	57/137	194
4	1000	71/172	243

Figure 1 (b) shows the transverse electric field distribution of 5DBR layers and incidence light wavelength (λ_c) of 800 nm. The bar diagram shows the intensity (1.988) of light within the DBR layers. Here, red and cyan colors were confirmed the strong light scattering/diffraction mechanism.

Further, the pink color shows less intensity of light.

3. RESULTS AND DISCUSSION

3.1. Photonic Band Gap Investigation

As compared to the various conventional materials, the photonic crystals are preferred due to the best light confinement among the air medium and selected materials. Furthermore, the radiation losses are zero at the sharp band edges [23-24]. Here, the photonic band gap diagram of the one-dimensional photonic crystals can adjust by changing the various structural parameters such as the each layer thickness, materials selection, and center wavelength of incident light. According to the photonic crystal theory, changing the center wavelength is proportionally equal to the resizing the band structure as shows in figure (2)-(5). Figure 2(a)-(b) depicted the reflectivity spectra and photonic band gap of 1D photonic crystals (Si/SiO₂). The reflectivity is enhanced with respect to the number of DBR layers. Under the center wavelength of 400 nm, the reflectance and photonic band gap varied from 300-570 nm as shown in table 2.

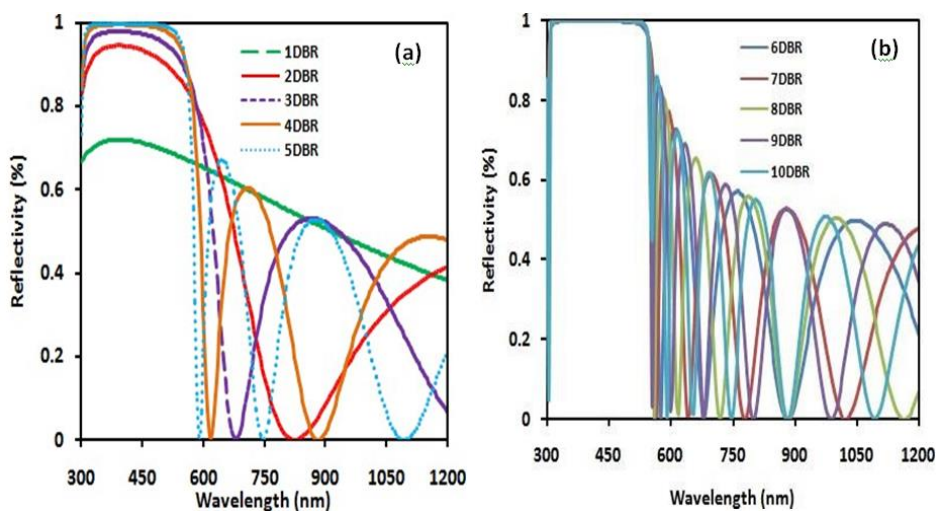


Fig. 2. The reflectivity of 400 nm center wavelength of 1DBR-10DBR structures.

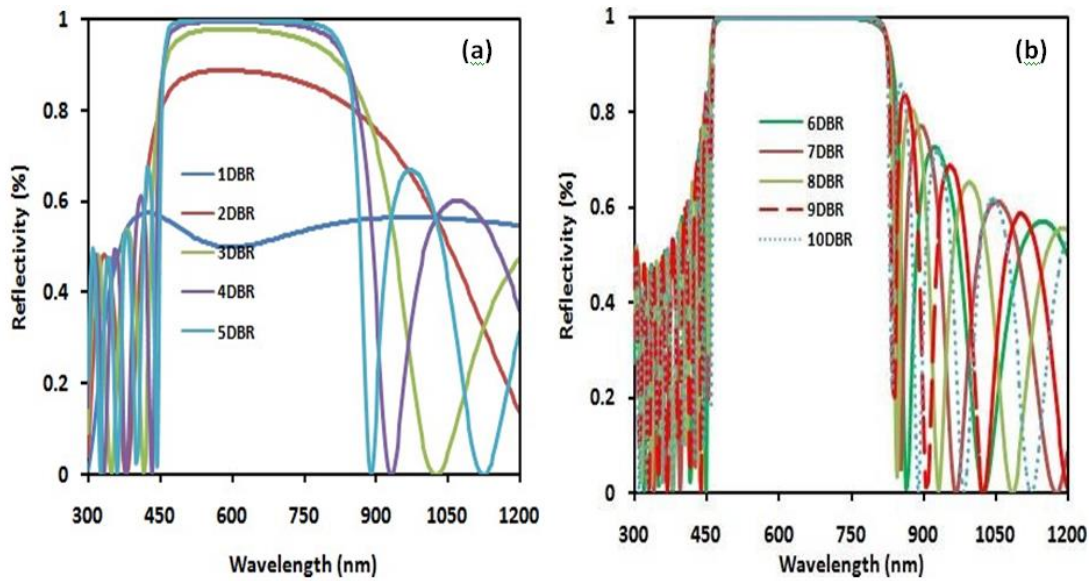


Fig. 3. The reflectivity of 600 nm center wavelength of 1DBR-10DBR structures.

Further, observed the enhancing the number of DBR stacks increased the oscillation of electromagnetic light waves is suppressed which helped to generate, the better and confinement of light within the band gap at the omnidirectional way [25]. However, we have varied the 1DBR to 10 DBR stacks and noticed the highest (or broader) reflectance with 99.9% started from 5DBR stacks.

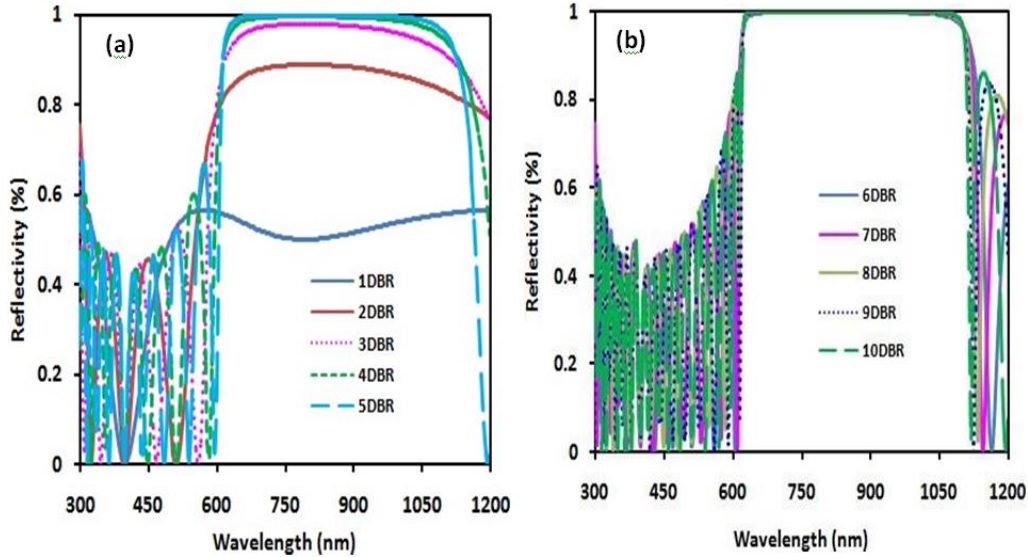


Fig. 4. The reflectivity of 800 nm center wavelength of 1DBR-10DBR structures.

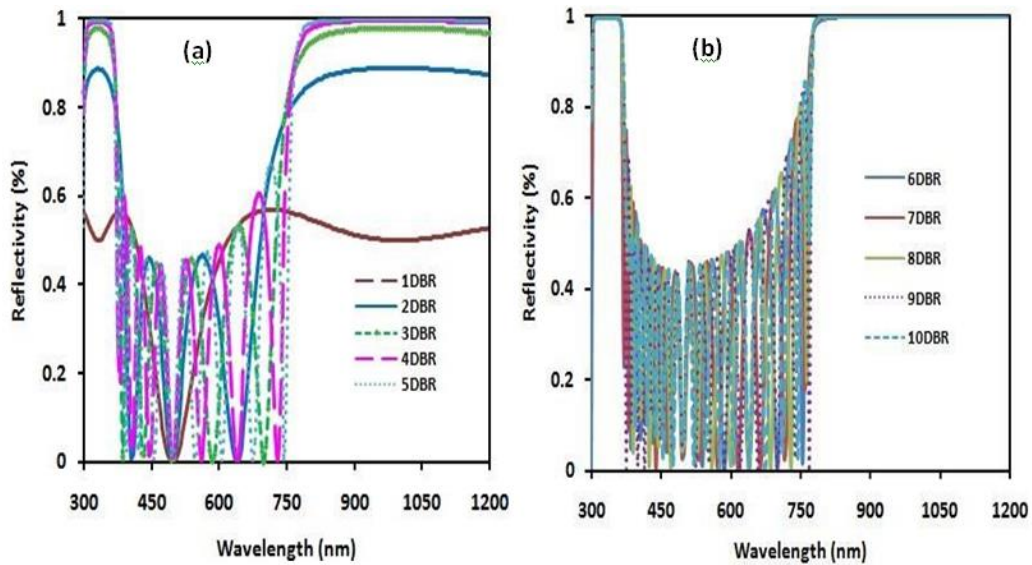


Fig. 5. The reflectivity of 1000 nm center wavelength at 1DBR-10DBR structures.

Figure 3 (a)-(b) shows the reflectance spectra of 1DBR to 10 DBR of Si/SiO₂ 1D photonic crystals under center wavelength of 600 nm. Overall, the total photonic band gap of 400 nm obtained from and varies from 455-855 nm. The improved, shifted and broader PBG achieved with the influence of the thickness of the DBR layers. In the photonic crystals, the transverse electric field guiding is accomplished by the distribution of reflected light within the 1D photonic crystals [24]. By employing plane wave method the photonic band gap calculated and studied their properties. *Saravanan and Dubey (2020)* reported the photonic band gap shifting towards the longer wavelength with respect to the increased number of 1D photonic crystal (DBR) layers [18]. Figure 4 (a)-(b) depicts the reflectance spectra of 1D photonic crystals of Si/SiO₂ alternative layers under 800 nm center wavelength. Totally, we have calculated the photonic band gap of 530 nm and vary from 615- 1145 nm. As compare others, the wide photonic band gap noticed under the center wavelength of 800 nm. *Saravanan and Dubey* experimentally reported the enhancement of a number of alternative layers (SiO₂/TiO₂) and generated the photonic band gap shifting towards the longer wavelength [20]. Furthermore, the reflectance study was enhanced with center wavelength of 1000 nm as shown in figure 5. The 1D photonic crystals of Si/SiO₂ layers varied from 1DBR-10DBR and found maximum reflectivity at 5DBR layers with 99.99%. The reflectivity starts from 760 nm and continuing the bandgap. Here, the reflectivity study was carried out from 300 to 1200 nm region.

Table 2. The Photonic band gap with respect to the center wavelength

Center Wavelength (nm)	Wavelength range (nm)	PBG (nm)
400	300-570	270
600	455-855	400
800	615-1145	530
1000	760- >1200	>440

The selected the optimal 5DBR layers and corresponding reflection spectra shows in figure 6 (a)-(b). Next, we calculated the photonic band gap of the 5 DBR layers as tabulated in table 2. Among various center wavelength, $\lambda_c=800$ nm shows wider photonic band gap due to the enhanced the center wavelength (nm) and shifting to the near-infrared region (refer fig. 10). These photonic band gap calculations determined by the Bragg's condition. This reflectivity investigation was carried out under normal incidence angle (0°) with air mass 1.5G.

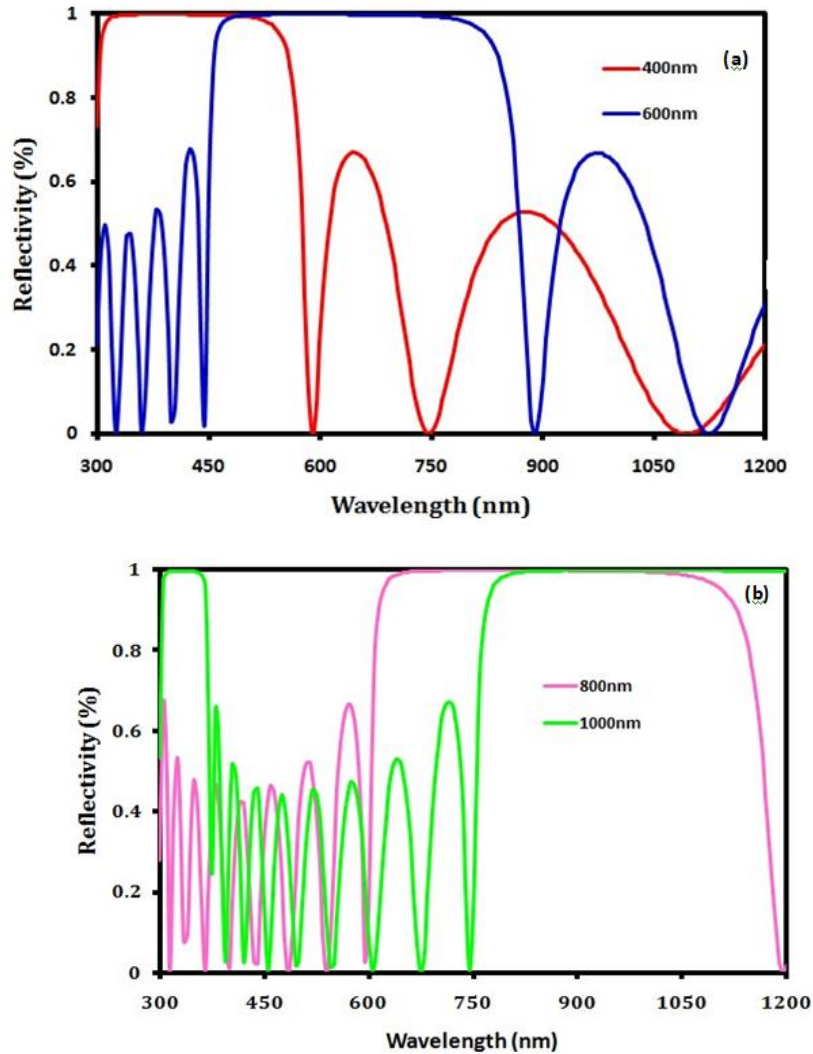


Fig. 6. (a) The reflectivity of center wavelength (a) $\lambda_c= 400$ & 600 nm (b) $\lambda_c= 800, 1000$ nm.

By incrementing the incident angle, the reflectivity was shifting towards the shorter wavelength region as reported by *Gondek and Karasinski (2012)* [25]. The resulting modulated structures were formed from multiple DBR layers of dielectric (Si/SiO₂) materials in which each layer partially reflects and transmitting the optical wave. The spectral wavelength range was calculated from 300 to 1200 nm. Beyond 1200 nm, the percentage of the solar spectrum absorption less and high energy losses noticed in solar cells due to unabsorbed photons as reported by *Joseph Day* [26]. *Saravanan and Dubey* experimentally reported the higher and broader reflectivity noticed due to the no. of alternative layers [20]. The broader PBG noticed with the effect of higher center wavelength with $\sim 100\%$ reflectivity [22]. The reflected waves combine and provide constructive

interference and the layers are acting as a perfect mirror back reflector. These DBR layer reflectivity (R) defined as,

$$R = \left[\frac{n_0(n_2)^{2N} - n_s(n_1)^{2N}}{(n_1)^{2N} + n_2(n_2)^{2N}} \right]^2 \quad (2)$$

where, 'n0' is the refractive index of the air (background) medium, 'n1' is the refractive index of the silicon, 'n2' is the refractive index of the SiO₂, 'ns' is the substrate refractive index and 'N' is the number of stacks (or repeated pairs) [27]. Moreover, when the 5DBR layers of the maximum reflectance reached up to 99.84% with a wider band gap. Within the reflected wave, the upper part ensures the highly reflected wave of short (400-600 nm) and longer (800 nm) wavelengths of light, thereby targeted sufficient broader reflectance.

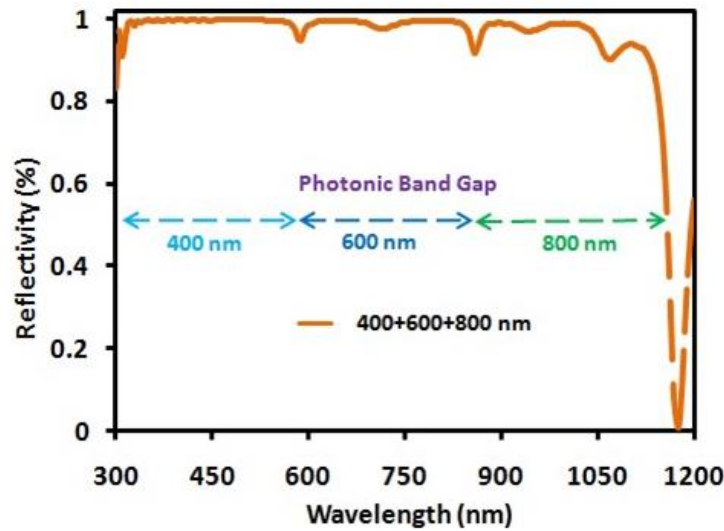


Fig. 7. The reflectivity of 15 DBRs (400+600+800 nm) structures.

The reflectivity of 15DBR (400+600+800nm) stacks is shown in figure 7. The wider photonic band gap noticed from 300 to 1150 nm spectral region. With the effect of various center wavelength combinations of DBR showed highest reflectivity in the UV-Visible and infrared region.

3.2. Amorphous Silicon Solar Cells (A-Si SC)

For the enhancement of light trapping mechanism, 5DBR with different center wavelength (λ_c) was integrated as a backside reflector in amorphous silicon solar cells, which includes ITO-anti-reflection coatings (20 nm), absorber (40 nm) and top-ITO nanogratings (nanogratings). Here, metallic/dielectric nanogratings are an effective approach in solar cells for the improvement of the light trapping mechanism [24]. Among these, the center wavelength (λ_c) of 400 and 800 nm DBRs integrated solar cell generated the less optical performance (5.43% and 4.88%) in longer wavelength.

The absorption spectra for 5 DBR (distributed Bragg's reflector) with nanogratings are generating the highest cell performance of 5.84 % under $\lambda_c=600$ nm center wavelength. The incidence light absorption records the total power of absorbed within the domain, such as periodic boundary condition (PBC, X- and Y-axis) and perfectly matched layer (PML, Z-axis). This domain reduces the unwanted light reflection, interaction and helps to collect the entire

incident light by increasing reflection or life time. The absorption was determined by $A(\lambda)=1-T(\lambda)-R(\lambda)$, here 'T' is the transmittance and 'R' is the reflectance. By considering plane wave incident on the solar cell, the reflectance and transmittance calculated by RCWA method which solves the electromagnetic field problem using Maxwell equations with PBC and PML boundary conditions [28-29]. The absorption has been depending on the length (or width), and height of the monitor. Further, this work extended by addition of 10DBR which includes any two different center wavelength 5DBRs. But, the center wavelength of 1000 nm was not considered the unabsorbed light photons. So the possible combinations of 10DBR stacks of $(400+600 \lambda_c)$, $(600+800\lambda_c)$, $(800+400\lambda_c)$ along with that the ARC and top-ITO gratings are integrated. Figure 8 shows the light absorption spectrum of two different center wavelengths (10DBR) integrated DBRs used as a backside reflector in thin film amorphous silicon solar cells. Further, this solar cell consists of ITO antireflection coating (ARC, 108 nm) layer, top-ITO (Gt, 20 nm) nanogratings and amorphous silicon (40 nm) absorber. Here, the periodic grating is 20 nm. In designing solar cell, the backside reflector consists of 10DBR(400+600)+Gt+ARC, 10DBR(400+800)+Gt+ARC, and 10DBR(600+800)+Gt+ARC. Next, the thicknesses of the each layerlike ARC and DBR stacks are determined by using the quarter wave criterion $(\lambda_c/4n)$, where ' λ_c ' is represented as center wavelength (400, 600 and 800nm) and 'n' is the refractive index of the materials.

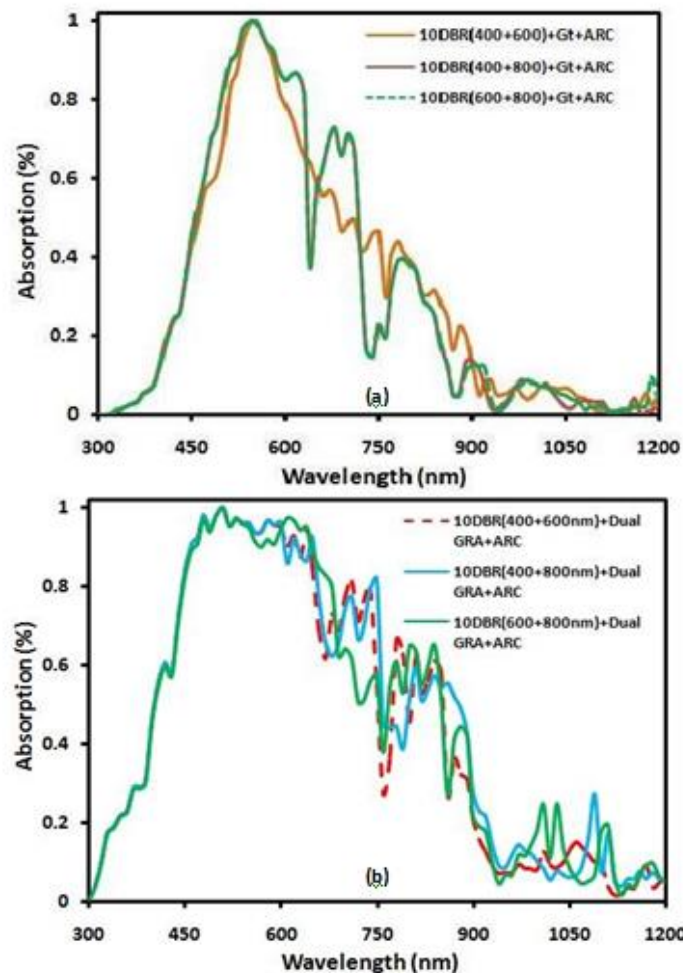


Fig. 8. Absorption spectra of two different center wavelengths combined without (a) and with (b) Bottom Ag grating solar cells.

In similar way, the no. of DBR increased approximately 10DBR that bottom 5DBR stacks center wavelength high and the top of that another 5 DBR stacks made by lowest center wavelength. We have compared two different center wavelength based multilayers (10DBR) combined in that maximum absorption (brown solid line) obtained by 10DBR(400+800)+Gt+ARC based solar cell structure as shown in Figure 8a. These solar cells are yielded the maximum 6.18% cell efficiency due to the enhanced absorption in the visible spectral region. Other DBR layers (combination of 400+600nm and 600+800nm) based solar cell produced 6.03% and 5.93% cell efficiencies. Further, the metallic-Ag asymmetrical nanogratings were added at the bottom of the absorber acts as a backside reflector with the 10DBR stacks in thin film amorphous silicon solar cells.

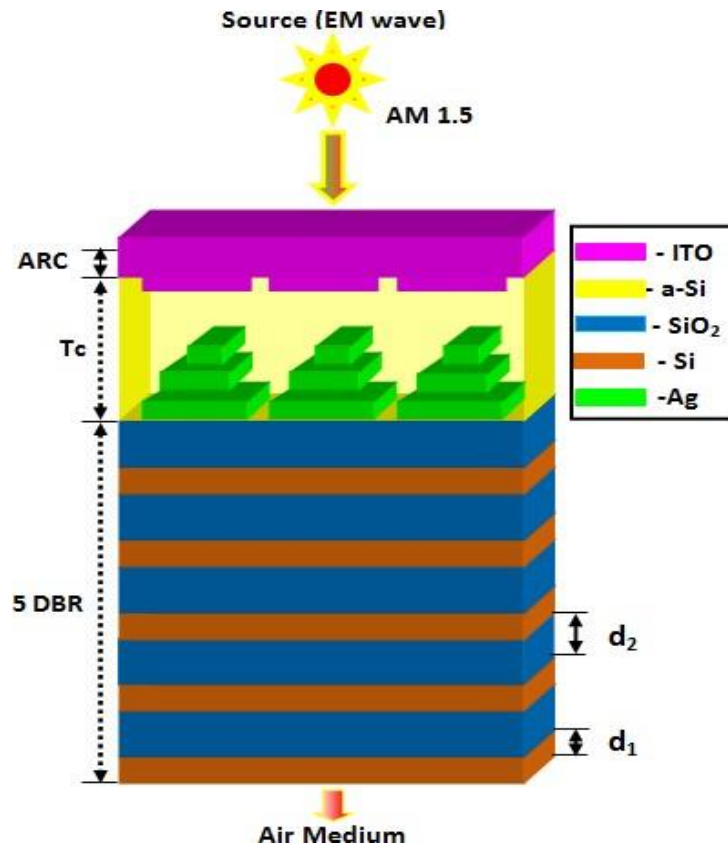


Fig. 9. The Schematic diagram of amorphous silicon solar cells.

Figure (8b) shows the absorption spectrum of amorphous silicon solar cells with the different center wavelengths. With the influence of asymmetrical nanogratings, the entire spectral region showed remarkable absorbance in the ultraviolet and visible spectral region due to the metallic nanogratings. When the thickness (d) of the DBR layers is increased the number of allowed modes also increasing.

Similarly, the photonic band gap is broadening with respect to the layer thickness as shown in table 2. The proposed solar cell structures are 10DBR(400+600)+Dual GRA+ARC, 10DBR(400+800)+Dual GRA+ARC and 10DBR(600+800)+Dual GRA+ARC. Generally, the asymmetrical Ag nanogratings provided omnidirectional scattering and diffraction with large angles. Overall, the enhancement of the collection of the light photons increased and generating improved electron-hole recombination. Among these solar cells, 10DBR(600+800)+Dual GRA+ARC structure showed (green solid line) cell efficiency of 16.08% and others (400+600nm and 400+800nm) achieved at 15.41%, 16.02%. Considerably, the absorption of the photon

increased in IR (>700nm) region due to the bottom asymmetrical Ag nanogratings. It has increased the cell efficiency due to the guided mode resonance (GMR) in the longer wavelength.

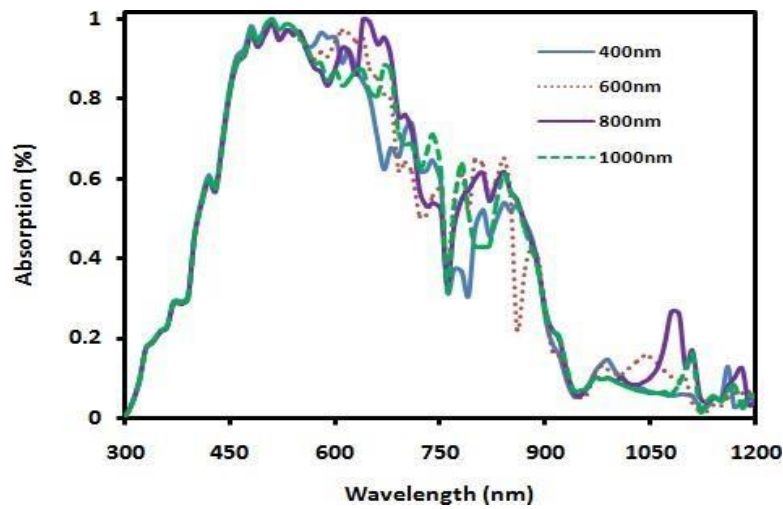


Fig. 10. The absorption spectrum of 5DBR integrated thin film amorphous silicon solar cells with various center wavelengths.

Figure 9 shows the schematic diagram of thin film amorphous silicon solar cell integrated with 5DBR (800 nm λ_c), ARC-ITO (108 nm), top-ITO nanogratings, amorphous silicon absorber (40 nm) and bottom-Ag asymmetrical nanogratings. The Ag-metallic and ITO-dielectric nanogratings thickness is 20 nm and distance ($D=20\text{nm}$) between the gratings are maintained. With the addition of dual gratings and 5DBR stacks the amorphous silicon solar cell performance was carried out by using various center wavelengths such as 400, 600, 800, and 1000 nm. The absorption (%) of amorphous silicon solar cells is shown in figure 10. As compared different solar cells, 5DBR of 800 nm center wavelength showed increased performance due to the high photonic band gap and further extending this investigation by changing the solar cell structures.

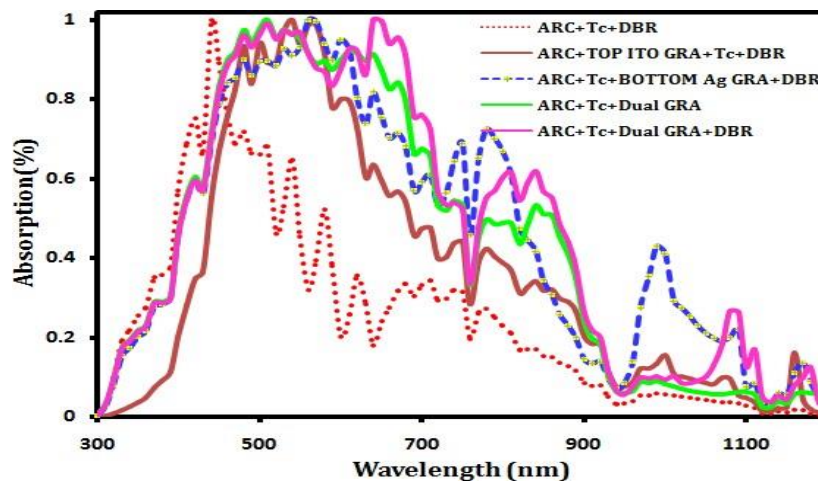


Fig. 11. Absorption spectra of solar cells with different structures.

Figure 11 depicts the absorption spectra of the complete solar cells with different back reflector under 800 nm center wavelengths (λ_c). It is seen that the absorption enhanced with dual grating with distributed Bragg's reflector (DBR) based ultra thin solar cells (solid line-pink). In this cell structure, the incident light when it has been reaching into the top-ITO grating, the incident light

spreading (allows), reducing the back reflection and diffracting the photons at various angles or direction.

Next, the bottom asymmetrical Ag-nanograting also important part to enhance in coupled light is further diffract and reflected back to the absorber layer (Yellow dotted line). Overall, dual the grating and DBR integrated based structure significantly broader and stronger performance in longer wavelength region. The periodicity in the lateral X-axis (direction), the incoming light coupled back into the absorber region by the reflectivity of DBR layers which is depends on the center wavelength and polarization conditions [16]. These structures are enabling a strong light-matter interaction due to that increased the photon absorption. Through these electric field profiles shows significantly enhance the guided mode between the gratings. However, the induced TE field is showing figure 12. To observe the best electric field distribution within the absorber region, we have simulated and optimized 1DPC as omnidirectional reflector used as a backside reflector in amorphous silicon solar cells.

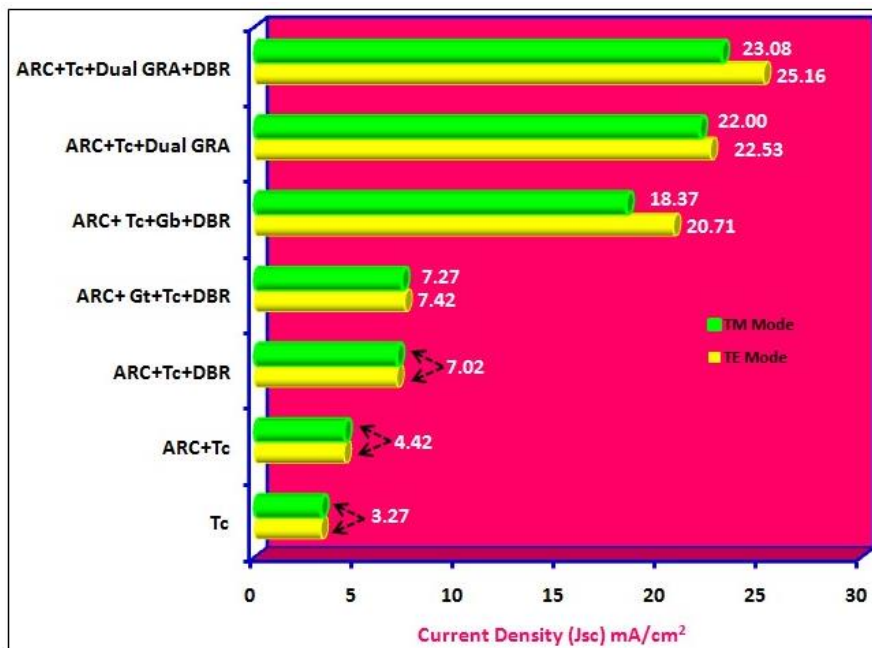


Fig. 12. The current density (Jsc) of various amorphous silicon solar cells.

The collection of the light photons enhanced with the 5DBR and dual gratings was integrated in solar cells and further the current density and electric field calculated. The current density (Jsc) also calculated by

$$J_{sc} = \frac{e}{hc} \int_{300}^{1200} \lambda(\lambda) \frac{dI}{d\lambda} d\lambda \quad (3)$$

here, 'λ' is the wavelength, 'c' is the speed of light, 'h' plank's constant, 'A' is the absorption in the absorber region, 'I' is the incident light spectrum (Wm⁻² nm⁻¹) [30]. Figure 12 shows the current density of amorphous silicon solar cells under the transverse electric (TE) and magnetic (TM) field polarization modes.

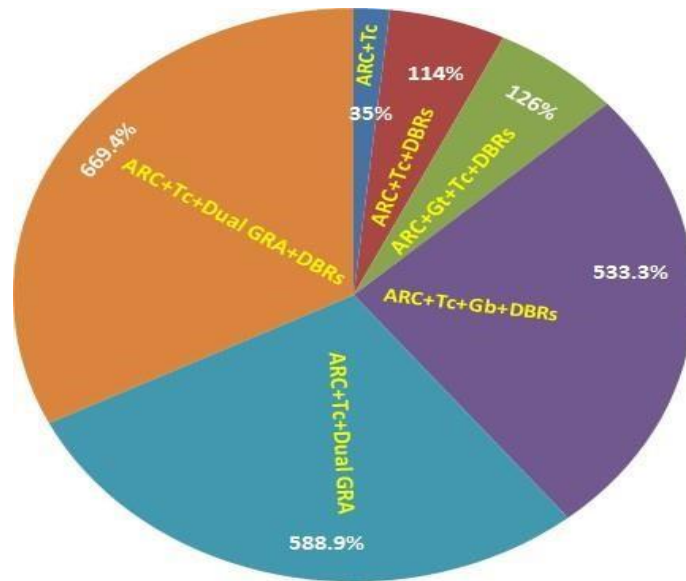


Fig. 13. The relative enhancement of current density (J_{sc} , mA/cm^2).

The absorber region (T_c) shows $3.27 \text{ mA}/\text{cm}^2$ in the both polarization conditions. Next, with the integration of ITO-ARC layer enhance the current density up to $4.42 \text{ mA}/\text{cm}^2$ and further 5DBR added as backside reflector and reached the current density (J_{sc}) maximum $7.02 \text{ mA}/\text{cm}^2$.

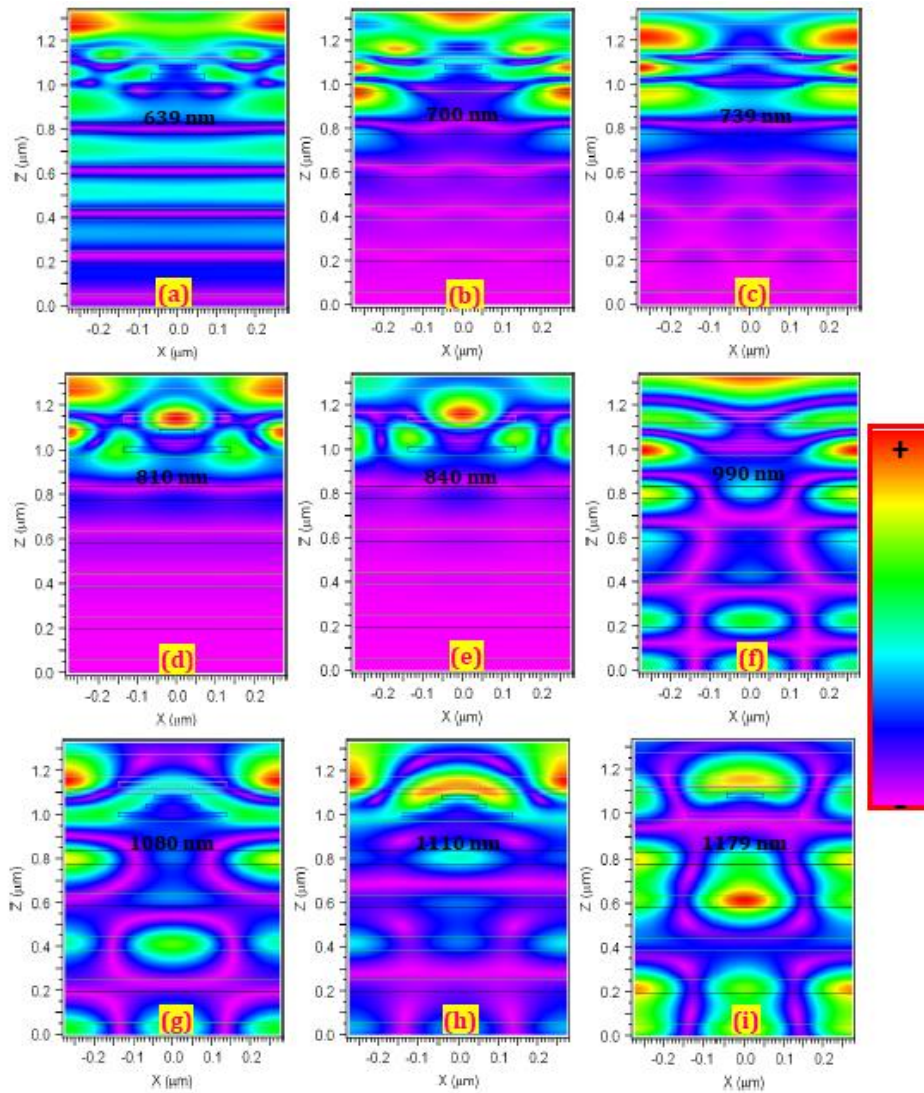


Fig. 14. Electric field (E_y) profiles for the amorphous silicon solar cells.

Further, top-ITO gratings added on the top of the amorphous silicon absorber region due to that $\sim 7.5 \text{ mA/cm}^2$ current density observed. Similarly, the bottom of the active region added asymmetrical Ag-nanogratings added (ARC+Tc+Gb+DBR) and noticed significant current density of 20.71 (TE) and $18.37 \text{ mA/cm}^2 \text{ (TM)}$. Because the light trapping mechanism such as scattering, diffraction and omni-directional reflection. Here, the photonic effects play a prominent role in solar cells like surface, guided modes, Fabry-Perot resonance (**figure 13**). Furthermore, we have improved the cell performance by dual gratings (top and bottom gratings) and removed DBR layers due to this issue again the current density reached up to 22.53 mA/cm^2 (TE case) and 22.00 (TM case). This enhancement was achieved with the effect of plasmonic assistance like surface excitation between the dielectric and metallic nanostructures, guided modes in the absorber region, localized surface plasmon on the bottom Ag-metallic gratings etc. Finally, we have designed solar cells with the combination of photonic and plasmonic nanostructures were integrated in amorphous silicon solar cell named as ‘**ARC+Tc+Dual+DBR**’. Remarkably, this proposed cell structure gained 25.16 and 23.08 mA/cm^2 within the 40 nm thick amorphous silicon absorber region which was not reported by the researchers. From figure V, the relative enhancement of 669.4% calculated by using reference solar cell (‘**Tc**’). The transverse

electric field polarization shows the significantly dominating performance in thin film amorphous silicon solar cells.

Table 3. The comparison of various solar cell performances with reduced absorber region.

Absorber	Thickness	No. of DBR Layers	η (%)	Jsc (mA/cm ²)	Ref.
c-Si	50 nm	DBR (SiO ₂ /a-Si)	14.93	22.71	[1]
c-Si	10 μ m	DBR (Si ₃ N ₄ /Si)	13.2	27.5	[31]
c-Si	2 μ m	DBR (c-Si/SiO ₂)	31.3	-	[32]
c-Si	41 nm	DBR (Si/SiO ₂)	16.8	19.69	[6]
c-Si	1 μ m	DBR (Si/SiO ₂)	20.95	24.51	[12]
Silicon	40 nm	DBR (a-Si/SiO ₂)	14.93	22.71	[33]
a-Si	40 nm	DBR (Si/SiO ₂)	-	25.16	Present work

The RCWA method is slices each layer of solar cells and maintaining the homogeneous light (TE/TM) propagation by using Fourier expansion. Next, the boundary conditions of PBC and PML used to form a matrix and RCWA has been utilized to study the light trapping mechanism in solar cells as reported by various researchers [28, 34-39]. In this section the interaction of a TE (transverse electric) polarized light with the various incident wavelengths at normal incidence angles. Figure 14 (a) shows the electric field distribution at 639 nm wavelengths, the diffraction pattern noticed in the absorber region and bottom metallic-Ag asymmetric structures. Further, top-ITO gratings are helping to spread the incident light into the absorber region. Here, the filed distribution and intensity decreasing at the lower DBR stacks. The red and cyan color shows the strong field intensity within the solar cells. Figure 14 (b) depicts the strong electric field at the end of the top-ITO gratings and wave-like nature appeared in the DBR layers ($\lambda=700$ nm). In DBR, the partial light reflects back into the absorber region and remaining transmitting towards the lower region. The surface guided mode shows in the absorber region as depicted in cyan color. But, the very low intensity of light noticed in the DBR layers. Figure 14 (c) depicts the surface guided modes, Fabry-Perot resonance modes and low field intensity observed at 739 nm. The wave-like nature increased in the DBR layers. The back reflector (metal/dielectric) prevents the light escaping from the back side and reflecting back completely. Figure 14 (d)-(e) shows the strong field in the ARC region and metallic gratings. The light interaction reduced at 810 and 840 nm incident spectral region. In the near infrared spectral region, the sharp absorption peaks noticed and reduced the collection of the photons. Similarly, the field intensity reduced considerably at 990, 1080, 1110 and 1179 nm as shows in figure 14 (f)-(i) due to the unabsorbed light photons which is to be focused. But guided modes enhanced in the longer wavelengths such as 1080, 1110 and 1179 nm [30]. Overall, these results shows dual grating structure induces the electron-hole recombination effect and brings a better light absorption in longer wavelength (figure 8(c)). The optimal performance of various designed solar cell structures compared in table-3 as reported by various researchers. The optimal values of structural and optical parameters are responsible for the better light confinement in the amorphous silicon absorber region. These 1D photonic crystals totally reflected and acts as a perfect reflector in the amorphous silicon solar cells.

4. CONCLUSIONS

In this paper, we studied the influence of DBR layers (backside reflector) in thin film amorphous silicon solar cells by changing various incident wavelengths. Using RCWA method, the optimized DBR stacks (5DBR & 10DBR), top-ITO and bottom-Ag nanogratings integrated in amorphous silicon solar cells. The DBR and Ag nanogratings showed an extremely low-loss and serve as a backbone of the device and reveals an unusual way of light reflectivity and scattering mechanism.

The light trapping and optical path length of the light photons increased which was helpful to prevent recombination losses of electron and hole pairs. The cell performance of 10DBR and 5DBR stacks based thin film solar cells were compared and observed later one enhanced significantly. With the influence of 5DBR and nanogratings achieved the current density 25.16 mA/cm² within 40 nm thick absorber. The electric field distribution attributed to the possibility of light scattering and guided modes of different incident wavelength. Finally, the 1D photonic crystals (Si/SiO₂) and diffractive ITO/Ag nanogratings combination is capable to improve light trapping mechanism in thin film solar cells. This engineering design can fulfill the future energy needs of a new generation of solar cells with low-cost.

REFERENCES

- [1] Rebecca Saive “Light trapping in thin silicon solar cells: A review fundamentals and technologies”, *Progress in Photovoltaics: Research and Applications*, 29 (10), 1125-1137 (2021)
- [2] H.L. Chen, A. Cattoni, R.D. Lepinau et al., “A 19.9%-efficient ultrathin solar cell based on a 205-nm-thick GaAs absorber and a silver nanostructured back mirror”, *Nature Energy*, 4 (9), 2019.
- [3] Z. Durmaz, S. Husein and R. Saive “Thin silicon interference solar cells for targeted or broadband wavelength absorption enhancement”, *Optics Express*, 29 (3), 4324-4337 (2021).
- [4] F.X. Abomo Abega, A.T. Ngoupo and J.M.B. Ndjaka “Numerical design of ultrathin hydrogenated amorphous silicon-based solar cell”, *International Journal of Photoenergy*, 1- 13 (2021).
- [5] Y. Fink, J.N. Winn, S. Fan, C. Chen, J. Michel, J.D. Joannopoulos, E.L. Thomas “A dielectric omnidirectional reflector”, *Science*, 282 (5394), 1679-82 (1998).
- [6] S. Saravanan and R.S. Dubey “Study of Al-Doped and Al/N Co-Doped TiO₂ Nanoparticles for Dye Sensitized Solar Cells” *Journal of Materials & Environmental Science (JMES)*, 11(1), 8-14 (2020).
- [7] S. Saravanan “Optical Pathlength Enhancement in Ultrathin Silicon Solar Cell Using Decorated Silver Nanoparticles on Aluminium Grating” *Nanosystems: Physics, Chemistry, Mathematics (NPCM)*, 11 (1), 86-91 (2020).
- [8] R.S. Dubey and S. Saravanan “Light Trapping Enhancement in Thin Film Silicon Solar Cells with Different Back Reflector” *International Journal of Electrical Components and Energy Conversion (IJECEC)*, 3(5), 83-87 (2017).
- [9] J. Du, Y. An, C. Zhang, C. Zhu, X. Li and D. Ma “Photonic design and electrical evaluation of dual-functional solar cells for energy conversion and display applications”, *Nanoscale Research Letters*, 14, 70-1-9 (2019).
- [10] R. S. Dubey, S. Saravanan and S. Kalainathan “Performance Evaluation of Thin Film Silicon Solar Cell Based on Dual Diffraction Grating” *Nanoscale Research Letters*, 8, 688-693 (2014).
- [11] Rahul Dewan and Dietmar Knipp “Light trapping in thin film silicon solar cells with integrated diffraction grating” *Journal of Applied Physics* 106, 074901-1-7 (2009).
- [12] Tahmineh Jalali, Impact of one-dimensional photonic crystal back reflector in thin-film c-Si solar cells on efficiency”, *Applied Physics A*, 124, 370-1-7 (2018).
- [13] A. Soman, A. Antony “Tunable and spectrally selective broadband reflector – Modulated photonic crystals and its application in solar cells”, *Solar Energy*, 162, 525-532 (2018).
- [14] W. Yu, X. Jia, Y. Long, L. Shen, Y. Liu, W. Guo and S. Ruan “Highly efficient semitransparent polymer solar cells with color rendering index approaching 100 using one- dimensional photonic crystal”, *ACS Appl. Mater. Interfaces*, 7 (18), 9920-9928 (2015).
- [15] X. Sheng, L.Z. Broderick, L.C. Kimerling “Photonic crystal structures for light trapping in thin-film Si solar cells: Modeling, process, and optimizations”, *Optics Communications*, 314, 41-47 (2014).

- [16] X. Sheng, S.G. Johnson, L.Z. Broderick, J. Michel and L.C. Kimerling “Integrated photonic structures for light trapping in thin-film Si solar cells”, *Applied Physics Letters*, 100, 111110- 1-3 (2012).
- [17] M.Y. Kuo, J.Y. Hsing, T.T. Chiu, C.N. Li, W.T. Kuo, T.S. Lay and M.H. Shih “Quantum efficiency enhancement in selectively transparent silicon thin film solar cells by distributed Bragg reflectors”, *Optics Express*, 20 (S6), A828-A835 (2012).
- [18] S. Saravanan, and R.S. Dubey “One-dimensional photonic crystals (Si/SiO₂) for ultrathin film crystalline silicon solar cells”, *Nanosystems: Physics, Chemistry, Mathematics*, 11 (2), 189-194 (2020).
- [19] D. Zhang, W. Hu, Y. Zhang, Z. Li, B. Cheng and G. Yang, “Experimental verification of light localization for disordered multilayers in the visible-infrared spectrum”, *Phys. Rev. B*, 50, 9810 (1984).
- [20] S. Saravanan, and R.S. Dubey “Fabrication and Characterization of TiO₂/SiO₂ multilayers using sol-gel spin coating method”, *Nanosystems: Physics, Chemistry, Mathematics*, 10 (1), 63-69 (2019).
- [21] V.A. Tolmachev, T.S. Perova “Design of one-dimensional composite photonic crystals with an extended photonic band gap”, *Journal of Applied Physics*, 99, 033507-1-5 (2006).
- [22] S. Saravanan, and R.S. Dubey “Ultraviolet and visible reflective TiO₂/SiO₂ thin films on silicon using sol-gel spin coater”, *Nanosystems: Physics, Chemistry, Mathematics*, 12 (3), 311-316 (2021).
- [23] L. Escoubas, J-J. Simon, P. Torchio, D. Duche, S. Vedraïne, W. Vervisch, J.L. Rouzo, F. Flory, G. Riviere, G. Yeabiyo and H. Derbal “Bringing some photonic structures for solar cells to the fore”, *Applied Optics*, 50 (9), C329-C339 (2011).
- [24] R.S. Dubey “Near field computation in 1D photonic crystal waveguides for TE polarization”, *Digest Journal of Nanomaterials and Biostructures*, 7(3), 893-898 (2012).
- [25] E. Gondek and P. Karasinski “1-D Photonic crystals for Photovoltaics”, *Photonics Letters of Poland*, 4 (2), 75-77 (2012).
- [26] Joseph Day, S. Senthilarasu and T.K.Mallick “Improving spectral modification for applications in solar cells: A review”, *Renewable Energy*, 132, 186-205 (2019).
- [27] C.J.R. Sheppard, “”, *Pure and Applied Optics: Journal of the European Optical Society Part A.*, 4 (5), 665 (1995).
- [28] Feifei Qin, haiming Zhang, Caixia Wang, Jingjing Zhang and Cong Guo “Anodic aluminum oxide nanograting for back light trapping in thin c-si solar cells” *Optics Communications*, 331, 325-329 (2014).
- [29] L. Zhao, Y.H. Zuo, C.L. Zhou, H.L. Li, H.W. Diao, W.J. Wang “A highly efficient light- trapping structure for thin-film silicon solar cells”, *Solar Energy*, 84, 110-115 (2010).
- [30] S. Saravanan, R.S. Dubey and S. Kalainathan “Design and analysis of thin film silicon solar cells using FDTD method”, *Procedia Materials Science*, 10, 301-306 (2015).
- [31] R.S. Dubey, K. Jhansirani, S. Singh “Investigation of solar cell performance using multilayer thin film structure (SiO₂/Si₃N₄) and grating”, *Results in Physics*, 7, 77-81 (2017).
- [32] P. Bermel, C. Luo, L. Zeng, L.C. Kimerling and J.D. Joannopoulos “Improving thin-film crystalline silicon solar cell efficiencies with photonic crystals”, *Optics Express*, 15 (25), 16986-17000 (2007).
- [33] S. Saravanan, R.S. Dubey, S. Kalainathan, M.A. More, D.K. Gautam “Design and optimization of ultrathin crystalline silicon solar cells using an efficient back reflector”, *AIP Advances*, 5, 057160-1-9 (2015).
- [34] C.H. Lin, K.M. Leung, T. Tamir “Modal transmission-line theory of three-dimensional periodic structures with arbitrary lattice configurations”, *J. Opt. Soc. Am. A*, 19, 2005-2017 (2002).
- [35] M.G. Mooharam, T.K. Gaylord, “Rigorous coupled-wave analysis of planar-grating diffraction”, *J. Opt. Soc. Am.* 71, 811-818 (1981).
- [36] M.G. Mooharam, T.K. Gaylord, “Rigorous coupled-wave analysis of metallic surface-relief gratings”, *J. Opt. Soc. Am. A*, 3, 1780-1787 (1986).
- [37] M. Niggemann, M. Glatthaar, A. Gombert, A. Hirsch, V. Wittwer “Diffraction gratings and buried nano-electrodes – architectures for organic solar cells”, *Thin solid Films*, 451-452, 619-623 (2004).
- [38] H. Sai, Y. Kanamori, K. Arafune, Y. Ohshita, M. Yamaguchi “Light trapping effect of submicron surface textures in crystalline Si solar cells”, *Prog. Photovoltaics*, 15, 415-423 (2007).
- [39] Y. Shi, X. Wang, W. Liu, T. Yang, F. Yang “Hybrid light trapping structures in thin-film silicon solar cells”, *J. Opt.* 16, 075706-1-7 (2014).